ACS Catalysis

Research Article

pubs.acs.org/acscatalysis

Enhancing Selective Photooxidation through Co−Nx-doped Carbon Materials as Singlet Oxygen Photosensitizers

Wenting Wu,[†] Qinggang Zhang,[†] Xiaokai Wang,[†] Congcong Han,[†] Xiaodong Shao,[†] Yixian Wang,[†] Jialiang Liu,[†] Zhongtao Li,[†] Xiaoqing Lu,[‡] and Mingbo Wu*[,†]

[†]State Key Laboratory of Heavy Oil Processing, School of Chemical Engineering, and [‡]College of Science, China University of Petroleum, Qingdao, Shandong 266580, People's Republic of China

Supporting Information

ABSTRACT: Singlet oxygen ($^1O_2$) is considered one of the most effective and selective oxygen agents. However, it is always obtained with the help of heavy atoms in the photosensitizers to sensitize $^3O_2$. Herein, metal−nitrogen (M−Nx) doped $^1O_2$ photosensitizers were readily prepared from metal−nitrogen complex. Their relative metal centers (e.g., Co) chelated with the N/C moiety (Co−Nx/C) provide the primary active sites for $^1O_2$ generation and selective oxidation. The structures of Co−Nx active sites are investigated by scanning and transmission electron microscopy and X-ray photoelectron, Fourier transform infrared, and X-ray absorption fine structure spectroscopy. Their functions for $^1O_2$ generation are confirmed by electrons spin resonance, $^1O_2$ emission, KSCN poisoning test, and H_2SO_4 etching test. These Co−Nx photosensitizers show excellent selective photooxidation abilities for 1,5-dihydroxynaphthalene after irradiation by a light-emitting diode lamp. After simple concentration and filtration, it is easy to obtain the pure product (juglone), which is confirmed by ^1H NMR spectroscopy. On the basis of density functional theory calculations, metal (e.g., Co) chelated with N/C moiety, especially for the Co−pyridinic N structure, could effectively reduce the singlet−triplet energy gap (ΔE_{ST}). It is speculated that this strategy for lowering ΔE_{ST} could benefit intersystem crossing from the singlet state to the triplet state and efficient sensitization of $^3O_2$ (triplet state) into $^1O_2$ for selective photooxidation.

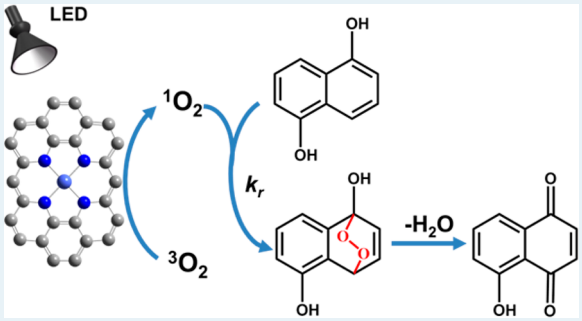

KEYWORDS: *Co−Nx/C, singlet oxygen, photooxidation, active site, DFT calculation*

1. INTRODUCTION

Energy shortage and environmental pollution are the main problems in the world today.[1] Thus, the need for a clean, renewable energy alternative is imminent.[2,3] On this basis, scientists have made great progress in photooxidation.[4−7] Reactive oxygen species (ROS) mainly include singlet oxygen ($^1O_2$), superoxide radicals ($O_2^{\bullet-}$), hydroxyl radicals ($^{\bullet}OH$), and hydrogen peroxide (H_2O_2), in which the $^1O_2$ is one of the most important ROS owing to its efficient and selective oxidation in wide applications such as photosensitization and photodynamic therapy.[8−11] Therefore, an efficient photosensitizer is required to sensitize the ground-state oxygen (triplet state, $^3O_2$) into singlet excited-state oxygen ($^1O_2$).[12] However, most $^1O_2$ is produced with the help of heavy atoms, such as iodine/bromine-containing organic dyes, transition metal complexes, and noble metal nanoparticles.[13−18] The heavy atom promotes the intersystem crossing (ISC) process of photosensitizers from singlet to triplet excited states and subsequently benefits the sensitization of $^3O_2$ into $^1O_2$. But the applications of these traditional photosensitizers are limited by poor selectivity, easy photobleaching, high cost, and biotoxicity. Therefore, it is better to find another way, such as reducing the singlet−triplet energy gap (ΔE_{ST}), to enhance the ISC process and $^1O_2$ generation.[8]

Metal−nitrogen (e.g., Co−N, Cu−N, or Ni−N) doped carbon materials, denoted M−Nx, show great potential for oxygen activation. First, M−N/C catalysts containing M−Nx active sites are easier to adsorb and activate the oxygen, in which it is possible to make great progress in catalysis.[19,20] For example, Co−Nx-doped carbon materials showed high activity for oxygen reduction reaction.[21,22] Then, metal ion chelated with the nitrogen complex in carbon materials, to some extent like metal porphyrins or metal phthalocyanines, may reduce ΔE_{ST} of carbon materials, which will benefit $^1O_2$ photosensitization.[23−25] Due to the proper elemental composition, inexpensive price, and easy chelation with metal, dimethylglyoxime is a good candidate for the fabrication of carbon materials with M−Nx active sites. As the metal ion chelates with the N atom of the ligand, it easily forms functionalized rigid structure that benefits the formation of M−Nx active sites during subsequent calcination.

In this work, Co−Nx/C sensitizers as representative were studied in detail. Co−Nx/C sensitizers were prepared from metal complex [Co(dmgH_2)(dmgH)Cl_2] (dmgH_2 = dimethyl-

Received: May 22, 2017
Revised: September 8, 2017
Published: September 11, 2017

DOI: 10.1021/acscatal.7b01671
ACS Catal. 2017, 7, 7267−7273

glyoxime) via facile one-step pyrolysis. Co−Nx active sites were confirmed by X-ray photoelectron (XPS), Fourier transform (FT-IR), and X-ray absorption fine structure (XAFS) spectroscopy. The introduction of Co−Nx active sites effectively enhances the generation of singlet oxygen and selective photooxidation activity of 1,5-dihydroxynaphthalene (1,5-DHN). The product (5-hydroxy-1,4-naphthalenedione, or juglone) is widely used in dyes, pharmaceutical synthesis, and hemostatic and antibacterial applications.[26−28] The active sites of activating oxygen molecules have been explored by H_2SO_4 etching and KSCN poisoning experiments for sensitized performance. Finally, density functional theoretical (DFT) calculations prove that the introduction of Co−Nx, (e.g., pyridinic N) can effectively reduce the singlet−triplet energy gap (ΔE_{ST}) and hence promote efficient selective $^1O_2$ generation. At the same time, it indicates that the effect of pyridinic N is better than that of pyrrolic N. This work provides a facile strategy for designing other similar $^1O_2$ photosensitizers and broadening the scope of application, such as photooxidation, wastewater treatment, and photodynamic therapy.

2. EXPERIMENTAL SECTION

2.1. Chemicals. All reagents of analytical grade or chemical grade were used without further purification. Dimethylglyoxime ($dmgH_2$, 98%) was purchased from Aladdin Industrial Corp. $CoCl_2·6H_2O$ (99%), $Ni(OAc)_2·4H_2O$ (98%), $Cu(OAc)_2·H_2O$ (98%), absolute ethanol (99.7%), and acetone (99.7%) were purchased from Sinopharm Chemical Reagent Co., Ltd.

2.2. Preparation of Cobalt Metal Complex. Cobalt metal complex was synthesized from $CoCl_2$ and dimethylglyoxime as in a previous report.[29] $CoCl_2·6H_2O$ (2.50 g) and dimethylglyoxime (2.75 g) were dissolved in 80 mL of acetone separately. These solutions were mixed and stirred for 5 min. Then the mixture was kept at room temperature for 24 h. Finally, a green precipitate of cobalt metal complex was obtained by further filtration, washing with acetone, and drying under vacuum; this material was named Co-cat. Preparation of nickel and copper metal complexes is described in Supporting Information.

2.3. Preparation of Co−Nx/C Sensitizers. Cobalt metal complex was then calcined at 300 °C for 2 h at a heating rate of 5 °C/min under N_2 atmosphere to avoid oxygen interference from air. Then, the block solid was ground into powder and washed three times with deionized water and absolute ethanol in a Soxhlet extractor. Finally, the block powder product was dried at 60 °C under vacuum; this material was named Co−Nx/C-300. Other products prepared by changing the calcination temperature (T = 250, 350, 400, or 500 °C) were named Co−Nx/C-T.

M−Nx/C sensitizers (M = Ni, Cu) were prepared at 300 °C under the same conditions as Co−Nx/C-300.

Co−Nx/C−H sensitizers were prepared from Co−Nx/C-300 (100 mg) immersed in 2 mol·L^{-1} H_2SO_4 at 70 °C for 3 h to remove the metal ions (H_2SO_4 immersion experiment).

Co−Nx/C-SCN sensitizers were prepared by poisoning with KSCN. Co−Nx/C-300 (100 mg) was immersed in 1 mol·L^{-1} KSCN at 60 °C for 3 h to poison Co−Nx active sites (poisoning experiment).

Cat-250 sensitizers were prepared by heating dimethylglyoxime (without metal) at 250 °C. It is hard to obtain sensitizers without metal under higher temperature, so the temperature 250 °C was selected instead of higher ones.

2.4. Photooxidation of 1,5-Dihydroxynaphthalene. An ethanol/water (1/1 v/v, 20 mL) mixed solvent containing DHN (1.0×10^{-4} M) and photosensitizer (Co−Nx/C, 15 mg) was put into a round-bottom flask (50 mL). The solution was irradiated with a light-emitting diode (LED) lamp at a power of about 10 W (light intensity = 120 W·m^{-2}) and constantly stirred. The LED lamp emits white light, and the excitation wavelengths are mainly 445 and 550 nm. UV−vis absorption spectra were recorded at intervals of 20 min. The consumption of DHN was monitored by decrease in the absorption peak at 298 nm, and the concentration of DHN was calculated from its molar extinction coefficient (ε = 7664 $M^{-1}·cm^{-1}$). Juglone production at intervals of 20 min was monitored by increase in the absorption peak at 419 nm. The concentration of juglone was also calculated from its molar extinction coefficient (ε = 3500 $M^{-1}·cm^{-1}$), and the yield of juglone was obtained from the concentration of juglone and the initial concentration of DHN.[16] The structure of the product was also confirmed by ^1H NMR.

2.5. Measurement and Characterization. The morphology and structure of the samples were characterized by transmission electron microscopy (TEM; JEOL JEM-2100UHR) and scanning electron microscopy (SEM; Hitachi S-4800). Further evidence for composition of the product was inferred from X-ray photoelectron spectroscopy (XPS), by use of an Escalab 250Xi spectrometer equipped with a prereduction chamber. Fourier transform infrared (FT-IR) spectra were recorded on a Nicolet 6700 spectrometer. UV−vis absorption spectra were measured on a UV−vis spectrophotometer (UV-2700, Shimadzu). Fluorescence spectra were measured on a spectrofluorometer (F-97 Pro, Shanghai Lengguang Technology Co., Ltd.). Electron spin resonance (ESR) spectra were recorded at room temperature on a JEOL JES FA200 spectrometer at 9.8 GHz X-band with 100 Hz field modulation. The $^1O_2$ emission signal of Co−Nx/C photosensitizer was detected on a fluorescence spectrometer (FLS980) with a 450 W Xe lamp and a near-infrared (NIR) detector. The sample was excited at 532 nm. The experimental conditions were excitation and emission bandwidths of 15 nm, integration time 2 s/step (0.1 s dwell time, 20 repeats), and step of 1 nm for the sample. All optical measurements were performed at room temperature. The $^1O_2$ trapping-ESR tests were performed by mixing sensitizers and 2,2,6,6-tetramethylpiperidine (TEMP; 1.0×10^{-2} M) in deionized water, and $O_2^{-\bullet}$ trapping-ESR tests were performed by mixing sensitizers and 5,5-dimethyl-1-pyrroline *N*-oxide (DMPO; 1.0×10^{-2} M) in methanol. Co K-edge XAFS measurements were performed at the Beijing Synchrotron Radiation Facility (BSRF). NMR spectra were obtained on a Bruker-300 spectrometer, at a frequency of 400 MHz for ^1H NMR, and the solvent was $CDCl_3$.

2.6. Hydroxyl Radical Detection. Coumarin as a fluorescence probe was dissolved in ethanol/water (1/1 v/v, 20 mL, c = 100 mg/L) and used for experiments. The fluorescent emission at 456 nm indicates the existence of $^\bullet$OH. The mixture of coumarin solution and Co−Nx/C (15 mg) was irradiated by a LED lamp for 20 min. Then fluorescence spectra were used to detect signals from the filtrate.[30]

2.7. Theoretical Calculations. The possible models for local and active structure were established on the basis of structural characterization. All theoretical calculations were obtained by means of Gaussian09.[31] DFT calculations with B3LYP/3-21G basis set were used for ground-state optimization of models. Energy levels of the S_n states (energy gap

DOI: 10.1021/acscatal.7b01671
ACS Catal. 2017, 7, 7267−7273

between S_0 and S_n) and T_n states (energy gap between S_0 and T_n) were calculated with time-dependent density functional theory (TD-DFT) calculations on the basis of optimized ground-state geometries.

3. RESULTS AND DISCUSSION

3.1. Preparation of Metal Complexes and Co−Nx/C Sensitizers. In order to prepare a photosensitizer with Co−Nx active site, it is necessary to select a suitable organic ligand that is quite easy to coordinate with a transition metal. Taking into account the price and capability of coordination of materials, we considered dimethylglyoxime as a potential organic ligand. Figure 1 shows the preparation of metal−organic complexes

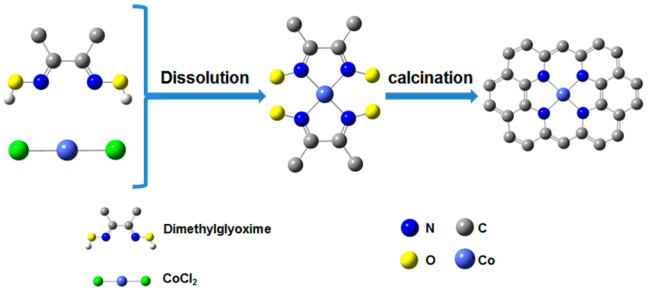

Figure 1. Schematic diagram for formation of Co−Nx/C photosensitizers (final product is shown as possible model structure of the metal active center).

and the relative M−Nx/C sensitizers. By changing the calcination temperature and the transition metal (Co, Cu, Ni), M−Nx/C sensitizers with different metal centers can be obtained. Herein Co−Nx/C sensitizers, as a representative example, were studied in detail. The active sites of activating molecular oxygen for Co−Nx/C sensitizers have been explored by NH_3 temperature-programmed desorption (TPD) and measurement of the sensitized performance.[19] Furthermore, the utility of Co−Nx as active sites for activating molecular oxygen was demonstrated by H_2SO_4 etching and poisoning experiments and theoretical calculations.[19]

3.2. Characterization of Co−Nx/C Sensitizers. The morphology and structure of Co−Nx/C-300 sensitizers were investigated by SEM and TEM. As shown in Figure 2a,b and Figure S1a, the synthesized Co−Nx/C-300 sensitizers exhibit a bulk structure. Elemental analysis mapping (Figure 2c−f)

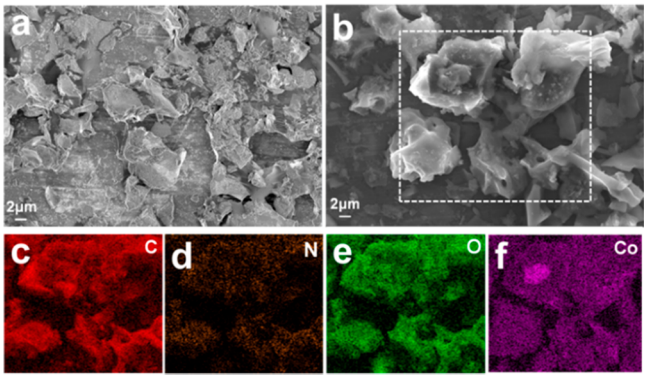

Figure 2. (a, b) SEM images of Co−Nx/C-300. (c−f) Corresponding elemental mapping images of (c) C, (d) N, (e) O, and (f) Co elements.

shows homogeneous distribution of C, N, O, and Co elements. The morphology was further confirmed by TEM (Figure S1b), which shows obvious clear bulk structure (gray oval). In addition, there are also some particulates or granular materials on the Co−Nx/C-300 sensitizers (Figure S1a). It may be inevitable to generate some Co_3O_4 nanoparticles or metal clusters during calcination. A high-resolution TEM image is shown in Figure S1c. Lattice spacing values of 0.21 nm can be assigned to the (111) planes of Co−Nx, and those of 0.24 nm can be assigned to the (311) planes of Co_3O_4.[32] Figure S2 shows UV−vis diffuse reflectance spectra (DRS) of Co−Nx/C sensitizers; they show broadband absorption from UV light to visible light.

In order to further prove the existence of Co−Nx, FT-IR spectra of Co−Nx/C sensitizers were measured and are shown in Figure S3. Compared with Cat-250 (no metal), all samples of Co−Nx/C sensitizers show new bands at 950−980 cm^{-1}, which can be assigned to Co−N stretching vibration, further confirming the formation of Co−Nx active sites in Co−Nx/C sensitizers.

X-ray photoelectron spectroscopy (XPS) was employed to accurately measure chemical composition and the content/type of N and Co on the surface of Co−Nx/C sensitizers. As shown in the XPS survey spectrum, there are C, N, O, Cl, and Co elements in Co−Nx/C-300 sensitizers (Figure S4a). High-resolution XPS spectra of Co and N were closely analyzed to explore the form of Co and N elements in the sensitizers. In the high-resolution Co 2p spectra of Co−Nx/C sensitizers (Figure 3a and Figure S4b,c), the peaks are fitted with two components

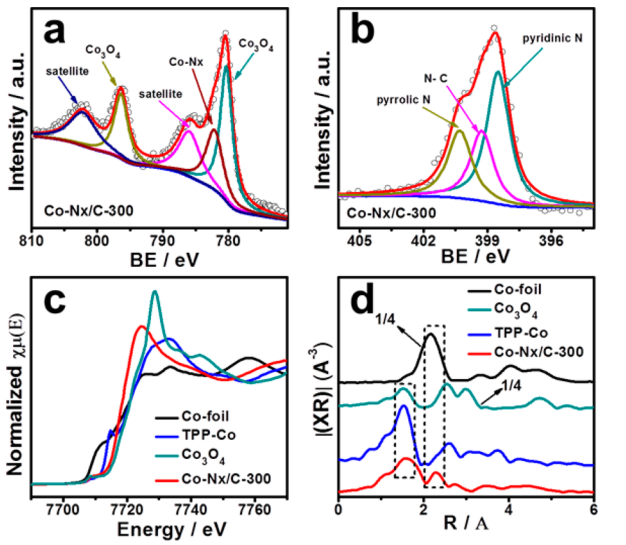

Figure 3. (a) XPS Co 2p spectrum of Co−Nx/C-300. (b) XPS N 1s spectrum of Co−Nx/C-300. (c) Normalized Co K-edge X-ray absorption near-edge structure (XANES) spectra of Co foil, Co−Nx/C-300, Co_3O_4 and TPP-Co (porphyrin cobalt). (d) Co K-edge EXAFS spectra of Co foil, Co−Nx/C-300, Co_3O_4, and TPP-Co.

corresponding to Co−Nx and Co_3O_4 peaks. The binding energy peaks at 780.1 and 796.5 eV can be attributed to Co_3O_4 peaks.[19,33] Furthermore, two satellite peaks at about 786.0 and 802.6 eV could be observed in the Co 2p spectra of Co−Nx/C sensitizers, which are characteristic peaks of cobalt oxides.[19] This indicates that some cobalt oxides are formed during pyrolysis. The peak at 782.2 eV can be assigned to Co−Nx.[19] The active component contents (Co−Nx) in Co−Nx/C

DOI: 10.1021/acscatal.7b01671
ACS Catal. 2017, 7, 7267−7273

sensitizers are summarized in Table S1. For Co−Nx/C-300, the Co−Nx content could reach 18.52 at. %, which is higher than that of Co−Nx/C-250 (15.79 at. %) and Co−Nx/C-350 (17.04 at. %). It is well-known that metal ions doped in the N/C moiety can more easily coordinate with oxygen molecule to activate oxygen.[19,34] Therefore, Co−Nx may be the active site of the sensitizers for oxygen activation (vide infra). From the high-resolution N 1s spectra of the Co−Nx/C sensitizers (Figure 3b and Figure S4d,e), three kinds of nitrogen at 398.6, 399.3, and 400.2 eV can be ascribed to pyridinic N, amine moieties (or other sp^3-C and nitrogen bonds), and pyrrolic N, respectively.[35] Pyridinic N is more likely to coordinate with Co and is considered as a possible active site in the reaction (vide infra). From Table S1, the percentage composition of pyridinic N in Co−Nx/C-300 (48.32 at. %) is obviously higher than that in Co−Nx/C-250 (38.50 at. %) and Co−Nx/C-350 (44.94 at. %) sensitizers. These results are in accordance with the Co XPS analysis. To some extent, this increasing content of Co−Nx active sites would benefit the photooxidation of Co−Nx/C-300.

X-ray absorption fine structure (XAFS) spectroscopy is a powerful approach to further study the valence state of metals and the structure of Co−Nx/C sensitizers at the atomic level.[36] XAFS can be divided into two parts, X-ray absorption near-edge structure (XANES) and extended X-ray absorption fine structure (EXAFS).[37,38] As shown in Figure 3c, the normalized Co K-edge XANES curves of Co−Nx/C-300 show that the near-edge absorption energy is located between those of Co foil and Co_3O_4, indicating that the valence state of cobalt ions in sensitizers follows the order Co_3O_4 > Co−Nx/C-300 > Co foil.[39] It is known that Co(II) porphyrin complexes (TPP-Co) contain a typical Co−N_4 coordination structure.[36] The EXAFS spectrum of Co−Nx/C-300 (Figure 3d) is similar to that of TPP-Co to some extent. The EXAFS curve for Co−Nx/C-300 shows a peak at 1.55 Å, close to that of TPP-Co, and it could be attributed to Co−N(O) scattering paths. Co−Nx/C-300 has another obvious peak at 2.26 Å. It is close to but larger than the Co−Co peak of Co foil, further indicating the existence of Co−N structure in this carbon material.

3.3. Detection of Reactive Oxygen Species. Selective $^1O_2$ generation is crucial for highly selective oxidation.[10] However, it is always confused by the presence of other ROS such as superoxide radical anion ($O_2^{-\bullet}$), hydroxyl radicals ($^\bullet$OH), and hydrogen peroxide (H_2O_2) during the molecular oxygen activation process.[10] To distinguish the $^1O_2$ performance from other ROS, electron spin resonance (ESR), chromogenic reaction of KI/CH_3COOH/starch system, and fluorescence techniques (coumarin as a probe molecule) were used to detect these ROS species. 2,2,6,6-Tetramethylpiperidine (TEMP) was selected as the trapping agent to prove the existence of $^1O_2$ in the sensitized system; this signal could be detected by ESR.[8,10,40] As shown in Figure 4a and Figure S5a,b, the ESR spectra of Co−Nx/C sensitizers clearly display a 1:1:1 triplet signal with g-value of 2.002, which is characteristic of 2,2,6,6-tetramethylpiperidine-N-oxyl (TEMPO).[8] Compared with Co−Nx/C-300, Cat-250 sensitizers exhibit negligible signal for TEMPO (Figure S5c). This indicates that introduction of the Co center is critical for $^1O_2$ generation. Furthermore, the characteristic $^1O_2$ emission from Co−Nx/C-300 appeared at 1265 nm (Figure 4b), which further confirms $^1O_2$ generation.[41]

H_2O_2 was detected by use of the KI/CH_3COOH/starch system.[42] A reddish-brown color was observed upon mixing the reaction system with KI/CH_3COOH/starch in the presence of

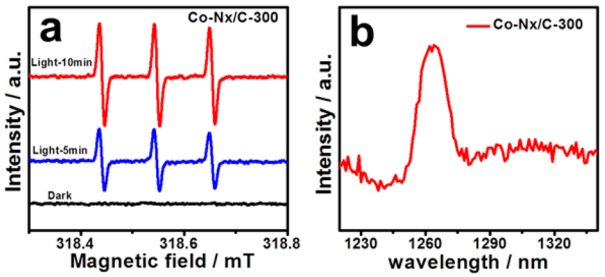

Figure 4. (a) ESR spectra of Co−Nx/C-300 upon irradiation for 10 min in the presence of TEMP. (b) $^1O_2$ emission of Co−Nx/C-300 under excitation with a 532 nm laser.

H_2O_2. Figure S6 shows that there is no H_2O_2 present in the reaction system.[42] Besides, 5,5-dimethyl-1-pyrroline-N-oxide (DMPO) was employed as scavenger for superoxide radical anion ($O_2^{-\bullet}$) in the system by ESR.[8] Figure S5d shows that there is a small amount of $O_2^{-\bullet}$ generation relative to $^1O_2$ generation from Co−Nx/C-300, but it hardly influences the selective oxidation. Next, hydroxyl radical ($^\bullet$OH) was explored by using a reactive probe molecule.[30] Coumarin as a probe molecule can react with $^\bullet$OH and form 7-hydroxycoumarin, which produces strong fluorescence intensity at 456 nm. Figure S5e,f shows no significant increase in fluorescence after 20 min of illumination, indicating that little $^\bullet$OH is produced in the reaction system.[30] As is known, $^\bullet$OH and $O_2^{-\bullet}$ are generated by a charge-transfer process that competes with the energy-transfer process corresponding to $^1O_2$ generation.[8] The presence of $^1O_2$ instead of $^\bullet$OH and $O_2^{-\bullet}$ in Co−Nx/C sensitizers suggests that energy transfer, rather than charge transfer, plays an important role for the Co−Nx/C sensitizers in photooxidation.

3.4. Photooxidation Activities. Owing to the high selectivity and efficiency for $^1O_2$ generation, Co−Nx/C sensitizers show promise to be excellent photosensitizers for selective oxidation reactions. In order to confirm the sensitizing abilities of Co−Nx/C sensitizers, 1,5-dihydroxylnaphthalene (DHN) was selectively converted to juglone (Figure 5a).[16] Upon irradiating the mixed solution of Co−Nx/C-300 and DHN with a LED lamp, absorption at 298 nm of DHN decreased and absorption at 419 nm (of the product juglone) increased (Figure 5b). The photooxidation reaction rate (k) of DHN and yield of juglone are summarized in Table S2 and Figure 5c. Among various photosensitizers prepared under different temperatures, Co−Nx/C-300 showed higher sensitized activity and higher selectivity; the product yield reached 32.29%. The crude product was dissolved in trichloromethane, and the pure product could be obtained by simple filtration. Other unreacted substances were mainly raw materials (DHN). In the blank experiment, UV−vis absorption intensity of DHN has almost no change without sensitizers after irradiation for 100 min (Figure S7a), and the amount of product juglone was negligible. Photooxidation of DHN was also explored in water/acetonitrile (1/1 v/v) mixed solvent under irradiation by LED lamp. As shown in Figure S7b, the product yield was 27.71%, which is very similar to the 32.29% yield in 1/1 water/ethanol. This indicates that ethanol is used as a solvent rather than as a sacrificial reagent. The dissolution of metal complex from Co−Nx/C-300 was explored in Figure S7c. Cobalt metal complex (Co-cat) exhibited a characteristic absorption peak at 250 nm. However, no absorption peaks were found in the filtrate of Co−Nx/C-300 in water/ethanol (1/1 v/v). Therefore, the

DOI: 10.1021/acscatal.7b01671
ACS Catal. 2017, 7, 7267−7273

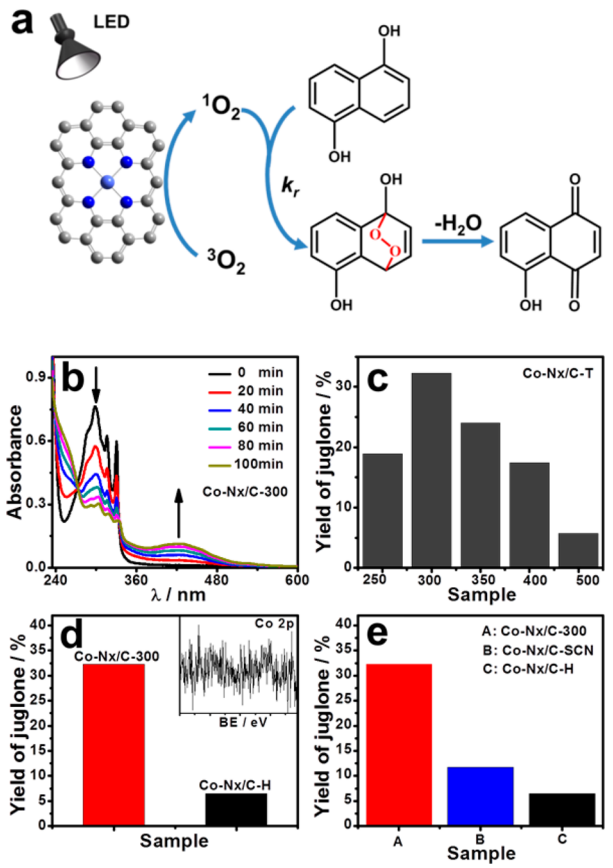

Figure 5. (a) Reaction mechanism diagram for photooxidation of DHN. (b) UV−vis absorption spectral changes for photooxidation of DHN (1.0×10^{-4} M) in H_2O/ethanol (1/1 v/v), *m*(Co−Nx/C-300) = 15 mg. (c) Yield of juglone for Co−Nx/C-*T* sensitizers. (d) Yield of juglone for Co−Nx/C-300 and Co−Nx/C-H (immersed in H_2SO_4 for 3 h). (Inset) XPS Co 2p spectrum of Co−Nx/C-300 sensitizers preleached in 2 mol·L^{-1} H_2SO_4 at 70 °C for 3 h. (e) Yield of juglone for Co−Nx/C-300, Co−Nx/C-SCN (poisoned by KSCN), and Co−Nx/C-H.

Co−Nx/C photosensitizer could not be dissolved in the solvent as a solid.

To further prove the structure and purity of juglone after reaction, the product was detected by ^{1}H NMR. As shown in Figure S8, the ^{1}H NMR spectrum of prepared product shows the same characteristic peaks as those of commercial juglone purchased from Aladdin Industrial Corp. The result indicates that no other byproducts are generated in this reaction. Because of the magnetism of cobalt metal in the sensitizers, it is easy to effectively separate sensitizers from reactants and products by magnetic separation technology (Figure S9).

On the basis of these results, Co−Nx has great possibility to be the active site for selective photooxidation. In order to confirm this, an etching experiment of Co−Nx/C-300 was carried out.[19] After immersion in 2 mol·L^{-1} H_2SO_4 at 70 °C for 3 h, there is little metal left (e.g., Co−Nx and Co_3O_4), which is confirmed by Co XPS (inset, Figure 5d). After this etching, the selective oxidation of Co−Nx/C-300 decreased sharply from 32.29% to only 6.50% (Figure S10a and Figure 5d). This demonstrates the important role of Co in the formation of active sites.[19]

To explore the species at the adsorption site, the chemisorption of NH_3 on sensitizers is investigated by temperature-programmed desorption (TPD).[19] As shown in Figure S11, a broad desorption peak can be observed in the temperature range 100−200 °C. According to the literature, the characteristic peak can be attributed to the weaker acidic sites, such as Co−Nx.[19] As is known, $^1O_2$ is generated through an energy-transfer process. Therefore, adsorption and activation of oxygen is one of the most important steps. To further prove it, small molecules (such as SCN^{1-}) were used to interrupt metal−O_2 adsorption by formation of highly stable metal−ligand coordination intermediate compounds.[19,43] After immersion in 1 mol·L^{-1} KSCN at 60 °C for 3 h to poison Co−Nx active sites, the sensitizing activity and selective oxidation of Co−Nx/C-300 decreased sharply (Figure 5e and Figure S10b). Figure S10c shows that almost no sensitizing activity can be observed for Co_3O_4 as a reference. These results show that Co−Nx acts as the primary active site in photooxidation. In this case, other metals (Cu, Ni) in the sensitizers were further explored, and the results show that M−Nx/C sensitizers provide a new strategy for enhancing selective oxidation (Figure S10d and Table S3).

3.5. Density Functional Theory Calculations. To further study the influence of Co−Nx active sites and pyridinic N on the generation of $^1O_2$, theoretical studies were performed by DFT calculations. On the basis of previous experimental analysis, four possible models are established by use of Gaussian09 (Figure S12), named PD-Co (Co−Nx with pyridinic N), PD (pyridinic N), PR-Co (Co−Nx with pyrrolic N), and PR (pyrrolic N). The ground-state geometries of the models were optimized by DFT methods with B3LYP/3-21G basis set. Then the energies of the singlet state (S_n) and triplet state (T_n) were also calculated by time-dependent density functional theory (TD-DFT). The metal center structures of bulk photosensitizers were speculated from experiment; to some extent, these energy-level calculations could reflect their relative energy gaps rather than the exact value. As shown in Figure 6 and Table S4, the major singlet excitation is $S_0 \rightarrow S_6$,

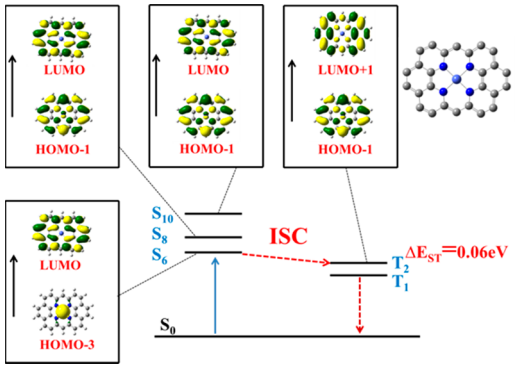

Figure 6. Selected frontier molecular orbitals involved in excitation and singlet/triplet excited states of PD-Co. (Left column) Singlet excited states (based on ground-state geometry); (right column) triplet excited states (based on ground-state geometry).

S_8, and S_{10}. The major electronic component of the $S_0 \rightarrow S_6$ transition is HOMO − 3 → LUMO, which can be assigned to electron transfer from metal to ligand. For triplet excitation ($S_0 \rightarrow T_1$ and $S_0 \rightarrow T_2$), the energy level of $S_0 \rightarrow S_6$ transition is closer to that of $S_0 \rightarrow T_2$, in which the major electronic component of the $S_0 \rightarrow T_2$ transition is HOMO − 1 → LUMO + 1.

The singlet−triplet energy gap (ΔE_{ST}) was calculated according to the excitation energy levels of singlet and triplet

DOI: 10.1021/acscatal.7b01671
ACS Catal. 2017, 7, 7267−7273

excited states. The S_n and T_n states originate from the same electronic configuration, so the energy gap between these states is consequently small. The smaller ΔE_{ST} favors the energy of intersystem crossing from singlet to triplet state, then it could be used to sensitize the $^3O_2$ (its ground state is triplet state) into $^1O_2$ through triplet−triplet energy transfer.[8] The calculation results are summarized in Figure 6, Figures S13−15, and Tables S4−S7. The PD-Co model has a smaller ΔE_{ST} (0.06 eV) than the PD model (0.30 eV). This result suggests that introduction of Co−Nx would favor intersystem crossing and hence efficient $^1O_2$ generation. Furthermore, ΔE_{ST} of PD-Co was also significantly lower than that of PR-Co, suggesting that pyridinic N plays a more active role in generation of $^1O_2$. At the same time, the percentage composition of pyrrolic N in Co−Nx/C-300 (25.88 at. %) is obviously less than that in Co−Nx/C-250 (35.78 at. %) and Co−Nx/C-350 (27.71 at. %) (Table S1). To some extent, it could be speculated that pyridinic N is the major factor in generation of $^1O_2$.

4. CONCLUSION

In summary, Co−Nx/C sensitizers were successfully prepared from cobalt metal−nitrogen complex via facile pyrolysis. The Co−Nx active sites are demonstrated by means of XPS, FT-IR, and EXAFS spectra. It is the first time that the introduction of Co−Nx active sites has effectively produced singlet oxygen and shown excellent selectivity in photooxidation of DHN. At the same time, introduction of Co−Nx active sites can effectively reduce the singlet−triplet energy gap (ΔE_{ST}), and hence efficient $^1O_2$ harvesting, according to DFT calculations. During the formation of Co−Nx active sites, the effect of pyridinic N is greater than that of pyrrolic N. Finally, via the introduction of other transition metals, this series of M−N/C sensitizers has been further explored for selective oxidation. This strategy offers new opportunities for developing the design of photosensitizers with selective efficient singlet oxygen generation.

■ ASSOCIATED CONTENT

Supporting Information

The Supporting Information is available free of charge on the ACS Publications website at DOI: 10.1021/acscatal.7b01671.

Additional text, 15 figures, and seven tables with characterization results, experimental details, and DFT calculation results (PDF)

■ AUTHOR INFORMATION

Corresponding Author

*(M.W.) E-mail wumb@upc.edu.cn.

ORCID

Wenting Wu: 0000-0002-8380-7904

Xiaoqing Lu: 0000-0002-7553-7131

Notes

The authors declare no competing financial interest.

■ ACKNOWLEDGMENTS

This work was financially supported by NSFC (51672309, 21302224, 51172285, 51372277, and 21572269), China Postdoctoral Science Foundation (2014M560590 and 2015T80758), Shandong Provincial Natural Science Foundation (ZR2013BQ028, ZR2013EMQ013, and ZR2014BQ012), Shandong Provincial Key Research Program (2015GSF121017), Project of Science and Technology Program for Basic Research of Qingdao (14-2-4-47-jch), and Fundamental Research Funds for Central Universities (15CX05010A, 15CX08005A and 15CX05013A).

■ REFERENCES

(1) Ong, W. J.; Tan, L. L.; Ng, Y. H.; Yong, S. T.; Chai, S. P. *Chem. Rev.* **2016**, *116*, 7159−7329.

(2) Rao, Y.; Wang, Y.; Ning, H.; Li, P.; Wu, M. B. *ACS Appl. Mater. Interfaces* **2016**, *8*, 33601−33607.

(3) Xie, M. Q.; Zhang, S. L.; Cai, B.; Huang, Y.; Zou, Y. S.; Guo, B.; Gu, Y.; Zeng, H. B. *Nano Energy* **2016**, *28*, 433−439.

(4) Li, Z. M.; Liu, C.; Abroshan, H.; Kauffman, D. R.; Li, G. *ACS Catal.* **2017**, *7*, 3368−3374.

(5) Wu, W. T.; Zhan, L. Y.; Fan, W. Y.; Song, J. Z.; Li, X. M.; Li, Z. T.; Wang, R. Q.; Zhang, J. Q.; Zheng, J. T.; Wu, M. B.; Zeng, H. B. *Angew. Chem., Int. Ed.* **2015**, *54*, 6540−6544.

(6) Shao, X. D.; Wu, W. T.; Wang, R. Q.; Zhang, J. Q.; Li, Z. T.; Wang, Y.; Zheng, J. T.; Xia, W.; Wu, M. B. *J. Catal.* **2016**, *344*, 236−241.

(7) Favron, A.; Gaufrès, E.; Fossard, F.; Phaneufl'Heureux, A. L.; Tang, N. Y.; Lévesque, P. L.; Loiseau, A.; Leonelli, R.; Francoeur, S.; Martel, R. *Nat. Mater.* **2015**, *14*, 826−832.

(8) Wang, H.; Jiang, S. L.; Chen, S. C.; Li, D. D.; Zhang, X. D.; Shao, W.; Sun, X. S.; Xie, J. F.; Zhao, Z.; Zhang, Q.; Tian, Y.; Xie, Y. *Adv. Mater.* **2016**, *28*, 6940−6945.

(9) Kearns, D. R. *Chem. Rev.* **1971**, *71*, 395−427.

(10) Wang, H.; Yang, X. Z.; Shao, W.; Chen, S. C.; Xie, J. F.; Zhang, X. D.; Wang, J.; Xie, Y. *J. Am. Chem. Soc.* **2015**, *137*, 11376−11382.

(11) Lu, W.; Xu, T.; Wang, Y.; Hu, H.; Li, N.; Jiang, X.; Chen, W. *Appl. Catal., B* **2016**, *180*, 20−28.

(12) Scurlock, R. D.; Wang, B. J.; Ogilby, P. R.; Sheats, J. R.; Clough, R. L. *J. Am. Chem. Soc.* **1995**, *117*, 10194−10202.

(13) Rey, Y. P.; Abradelo, D. G.; Santschi, N.; Strassert, C. A.; Gilmour, R. *Eur. J. Org. Chem.* **2017**, *2017* (15), 2170−2178.

(14) Ma, Z. F.; Zhang, M. C.; Jia, X. D.; Bai, J.; Ruan, Y. D.; Wang, C.; Sun, X. P.; Jiang, X. *Small* **2016**, *12*, 5477−5487.

(15) Chen, Y. Z.; Wang, Z. U.; Wang, H. W.; Lu, J. L.; Yu, S. H.; Jiang, H. L. *J. Am. Chem. Soc.* **2017**, *139*, 2035−2044.

(16) Wu, W. T.; Yang, P.; Ma, L.; Lalevée, J.; Zhao, J. Z. *Eur. J. Inorg. Chem.* **2013**, *2*, 228−231.

(17) Sun, J.; Zhong, F.; Yi, X.; Zhao, J. Z. *Inorg. Chem.* **2013**, *52*, 6299−6310.

(18) Wu, W. H.; Sun, J.; Cui, X.; Zhao, J. Z. *J. Mater. Chem. C* **2013**, *1*, 4577−4589.

(19) Yang, C. Q.; Fu, L. L.; Zhu, R. L.; Liu, Z. G. *Phys. Chem. Chem. Phys.* **2016**, *18*, 4635−4642.

(20) Chen, X. Q.; Yu, L.; Wang, S. H.; Deng, D. H.; Bao, X. H. *Nano Energy* **2017**, *32*, 353−358.

(21) Wei, J.; Hu, Y. X.; Wu, Z. X.; Liang, Y.; Leong, S.; Kong, B.; Zhang, X. Y.; Zhao, D. Y.; Simon, G. P.; Wang, H. T. *J. Mater. Chem. A* **2015**, *3*, 16867−16873.

(22) Kattel, S.; Atanassov, P.; Kiefer, B. *Phys. Chem. Chem. Phys.* **2013**, *15*, 148−153.

(23) Zhu, Q. Q.; Igarashi, M.; Sasaki, M.; Miyamoto, T.; Kodama, R.; Fukushima, M. *Appl. Catal., B* **2016**, *183*, 61−68.

(24) Dąbrowski, J. M.; Pucelik, B.; Regiel-Futyra, A.; Brindell, M.; Mazuryk, O.; Kyzioł, A.; Stochel, G.; Macyk, W.; Arnaut, L. G. *Coord. Chem. Rev.* **2016**, *325*, 67−101.

(25) Galstyan, A.; Riehemann, K.; Schafers, M.; Faust, A. *J. Mater. Chem. B* **2016**, *4*, 5683−5691.

(26) Novotná, P.; Pacáková, V.; Bosáková, Z.; Štulík, K. *J. Chromatogr. A* **1999**, *863*, 235−241.

(27) Yamashita, M.; Kaneko, M.; Tokuda, H.; Nishimura, K.; Kumeda, Y.; Iida, A. *Bioorg. Med. Chem.* **2009**, *17*, 6286−6291.

(28) Kot, M.; Karcz, W.; Zaborska, W. *Bioorg. Chem.* **2010**, *38*, 132−137.

DOI: 10.1021/acscatal.7b01671
ACS Catal. 2017, 7, 7267−7273

(29) Xu, Y. X.; Ye, Y.; Liu, T. F.; Wang, X. L.; Zhang, B. Q.; Wang, M.; Han, H. X.; Li, C. *J. Am. Chem. Soc.* **2016**, *138*, 10726−10729.
(30) Ishibashi, K.-i.; Fujishima, A.; Watanabe, T.; Hashimoto, K. *Electrochem. Commun.* **2000**, *2*, 207−210.
(31) Wu, W. T.; Wu, X. Y.; Zhao, J. Z.; Wu, M. B. *J. Mater. Chem. C* **2015**, *3*, 2291−2301.
(32) Li, J. S.; Zhou, Z.; Liu, K.; Li, F. Z.; Peng, Z. G.; Tang, Y. G.; Wang, H. Y. *J. Power Sources* **2017**, *343*, 30−38.
(33) Aijaz, A.; Masa, J.; Rösler, C.; Xia, W.; Weide, P.; Botz, A. J.; Fischer, R. A.; Schuhmann, W.; Muhler, M. *Angew. Chem., Int. Ed.* **2016**, *55*, 4087−4091.
(34) Chen, Y.; Zhao, S. F.; Liu, Z. G. *Phys. Chem. Chem. Phys.* **2015**, *17*, 14012−14020.
(35) Chen, P.; Xiao, T. Y.; Qian, Y. H.; Li, S. S.; Yu, S. H. *Adv. Mater.* **2013**, *25*, 3192−3196.
(36) Liu, W. G.; Zhang, L. L.; Yan, W. S.; Liu, X. Y.; Yang, X. F.; Miao, S.; Wang, W. T.; Wang, A. Q.; Zhang, T. *Chem. Sci.* **2016**, *7*, 5758−5764.
(37) Yang, W. X.; Liu, X. J.; Chen, L.; Liang, L.; Jia, J. B. *Chem. Commun.* **2017**, *53*, 4034−4037.
(38) Zhao, Y. F.; Chen, G. B.; Bian, T.; Zhou, C.; Waterhouse, G. I. N.; Wu, L. Z.; Tung, C. H.; Smith, L. J.; O'Hare, D.; Zhang, T. R. *Adv. Mater.* **2015**, *27*, 7823.
(39) Wang, X. Y.; Liu, Y.; Zhang, T. H.; Luo, Y. J.; Lan, Z. X.; Zhang, K.; Zuo, J. C.; Jiang, L. L.; Wang, R. H. *ACS Catal.* **2017**, *7*, 1626−1636.
(40) Nosaka, Y.; Natsui, H.; Sasagawa, M.; Nosaka, A. Y. *J. Phys. Chem. B* **2006**, *110*, 12993−12999.
(41) Ge, J. C.; Lan, M. H.; Zhou, B. J.; Liu, W. M.; Guo, L.; Wang, H.; Jia, Q. Y.; Niu, G. L.; Huang, X.; Zhou, H.; Meng, X. M.; Wang, P. F.; Lee, C. S.; Zhang, W. J.; Han, X. D. *Nat. Commun.* **2014**, *5*, No. 4596.
(42) Wang, R. Q.; Geng, Y.; Zhang, L. L.; Wu, W. T.; Fan, W. Y.; Li, Z. T.; Wang, L. Z.; Zhan, L. Y.; Wu, X. Y.; Wu, M. B. *Chin. J. Chem.* **2015**, *33*, 1251−1258.
(43) Wang, Q.; Zhou, Z. Y.; Lai, Y. J.; You, Y.; Liu, J. G.; Wu, X. L.; Terefe, E.; Chen, C.; Song, L.; Rauf, M.; Tian, N.; Sun, S. G. *J. Am. Chem. Soc.* **2014**, *136*, 10882−10885.

DOI: 10.1021/acscatal.7b01671
ACS Catal. 2017, 7, 7267−7273